JACS
JOURNAL OF THE AMERICAN CHEMICAL SOCIETY
pubs.acs.org/JACS
Article

Enabling *In Vivo* Photocatalytic Activation of Rapid Bioorthogonal Chemistry by Repurposing Silicon-Rhodamine Fluorophores as Cytocompatible Far-Red Photocatalysts

Chuanqi Wang,[#] He Zhang,[#] Tao Zhang, Xiaoyu Zou, Hui Wang, Julia E. Rosenberger, Raghu Vannam, William S. Trout, Jonathan B. Grimm, Luke D. Lavis, Colin Thorpe, Xinqiao Jia,* Zibo Li,* and Joseph M. Fox*

Cite This: *J. Am. Chem. Soc.* 2021, 143, 10793−10803

ABSTRACT: Chromophores that absorb in the tissue-penetrant far-red/near-infrared window have long served as photocatalysts to generate singlet oxygen for photodynamic therapy. However, the cytotoxicity and side reactions associated with singlet oxygen sensitization have posed a problem for using long-wavelength photocatalysis to initiate other types of chemical reactions in biological environments. Herein, silicon-Rhodamine compounds (SiRs) are described as photocatalysts for inducing rapid bioorthogonal chemistry using 660 nm light through the oxidation of a dihydrotetrazine to a tetrazine in the presence of *trans*-cyclooctene dienophiles. SiRs have been commonly used as fluorophores for bioimaging but have not been applied to catalyze chemical reactions. A series of SiR derivatives were evaluated, and the Janelia Fluor-SiR dyes were found to be especially effective in catalyzing photooxidation (typically 3%). A dihydrotetrazine/tetrazine pair is described that displays high stability in both oxidation states. A protein that was site-selectively modified by *trans*-cyclooctene was quantitatively conjugated upon exposure to 660 nm light and a dihydrotetrazine. By contrast, a previously described methylene blue catalyst was found to rapidly degrade the protein. SiR-red light photocatalysis was used to cross-link hyaluronic acid derivatives functionalized by dihydrotetrazine and *trans*-cyclooctenes, enabling 3D culture of human prostate cancer cells. Photoinducible hydrogel formation could also be carried out in live mice through subcutaneous injection of a Cy7-labeled hydrogel precursor solution, followed by brief irradiation to produce a stable hydrogel. This cytocompatible method for using red light photocatalysis to activate bioorthogonal chemistry is anticipated to find broad applications where spatiotemporal control is needed in biological environments.

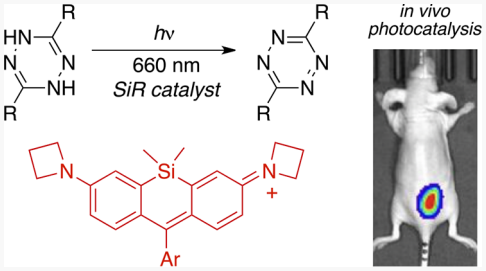

INTRODUCTION

Photocatalysis has had a transformative impact on organic synthesis and holds promise as an enabling tool in chemical biology and medicine.[1−4] To be useful for *in vivo* applications, it is generally necessary to initiate photochemistry in the far-red/near-infrared (NIR) window spanning 650−900 nm.[5] While red/NIR light is not toxic and can penetrate tissue, low energy (<45 kcal/mol) limits the modes of reactivity that can be initiated by photons at these long wavelengths.[5] Innovative strategies based on cyanine,[6] BODIPY,[7] and phthalocyanine dyes[8] and Ru complexes[9] have been used to initiate decaging with red/NIR light. In addition to these stoichiometric processes, NIR dyes have served as photocatalysts in photodynamic therapy (PDT), where O_2 and light are used to produce singlet oxygen, which causes oxidative damage and ultimately leads to cell death.[10] While photocatalytically generated singlet oxygen can be used to promote selected *in vivo* reactions,[11] for many applications the cytotoxicity and side reactions associated with singlet oxygen sensitization pose challenges for using long-wavelength photocatalysis to initiate many types of chemical reactions in biological environments.

Over the past two decades, bioorthogonal chemistry has been used for a broad array of applications spanning biomedicine and biotechnology.[12,13] A range of non-natural reactions can now be carried out routinely in live cells under *in vitro* or *in vivo* conditions not only for bioconjugation but also in deconjugative bioorthogonal reactions that enable cargo delivery.[14−22] Significant in this field has been the development of photoinducible bioorthogonal reactions as methods for turning on bioorthogonal reactions with spatial resolution and temporal control.[23,24] Important advances include photochemical reactions of tetrazoles[25−27] and cyclopropenone[28−31] derivatives to

Received: May 29, 2021
Published: July 12, 2021

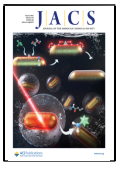

https://doi.org/10.1021/jacs.1c05547
J. Am. Chem. Soc. 2021, 143, 10793−10803

produce reactive nitrile imines and cyclooctyne derivatives, respectively. Other advances include photoinduced versions of the Staudinger[32] and CuAAC[33] reactions as well as cycloadditions involving azirines,[34] benzyne,[35] diarylsydnones,[36,37] quinones,[38−41] *o*-naphthaquinone methides,[42] *o*-quinodimethanes,[43,44] and *trans*-cycloheptene.[45] While several methods for initiating bioorthogonal chemistry using NIR light with two-photon excitation have been described,[29,46] prior to our work, the direct use of red/NIR light to induce bioorthogonal reactivity had not been described.[47]

The bioorthogonal Diels−Alder reactions of tetrazines with strained alkene and alkyne dienophiles have become increasingly important to the chemical biology community due to their exceptional kinetics with rates that can exceed 10^6 M^{-1} s^{-1} with conformationally strained *trans*-cyclooctenes.[48−51] Recent interest in the development of photochemically inducible variants of tetrazine ligation have prompted the discovery of new methods for uncaging cyclopropene[52,53] and bicyclononyne[28] dienophiles. Tetrazine (Tz) synthesis is commonly achieved through the oxidation of dihydrotetrazine (DHTz) precursors,[54] and the DHTz/Tz redox couple has been used in electrochemically controlled bioconjugation at electrode surfaces,[55] in batteries,[56] and for colorimetric nitrous gas detection.[57] In a preprint, an *o*-nitrophenylphenyl-protected dihydrotetrazine has been used with 405 nm light and without catalysis to uncage tetrazines that react with TCO with rates of 10^2 M^{-1} s^{-1}.[58]

An area of interest has been the development of hydrogel materials for disease modeling *in vitro* and cell delivery to specific anatomical locations *in vivo*.[59−61] In addition to physical cross-linking through non-covalent interactions,[62] gelation through covalent bond formation has been achieved via reactions including Michael additions,[63] click chemistry,[64] and photoinitiated cross-linking processes.[65] Photoinitiated methods of hydrogelation offer the additional benefit of precise spatial and temporal control. For *in vivo* applications, methods based on long-wavelength light[66,67] are desirable to enable deep tissue penetration. Such methods may extend to materials for regenerative medicine[68] and for *in vivo* disease modeling.[69,70] Injectable materials that can form 3D hydrogels have the potential for creating better cancer xenograft models for the study of cancer biology. For example, LNCaP prostate cancer cells are poorly tumorigenic and generally require other types of cells or Matrigel to support tumor model generation.[71,72] Two-photon methods provide an approach for hydrogel patterning with high spatial resolution using far-red/NIR light. However, the very small focal volumes of two-photon techniques can limit their biomedical applications, and the development of chemical methods that directly utilize far-red/NIR light would be desirable.[73]

Previously, our group described a method for catalytic turn-on of the tetrazine ligation, where rapid bioorthogonal reactivity can be induced by controllable, catalytic stimuli.[47] Either visible light and a photosensitizer or very low loadings of horseradish peroxidase can be used to catalyze the oxidation of a dihydrotetrazine to a tetrazine with oxygen as the terminal oxidant (Figure 1). Several photocatalysts were found to be effective including methylene blue, which catalyzes photooxidation with excitation by 660 nm light.

Our initial system for photocatalytic oxidation has found several applications,[74−76] including the activation of polymeric fibers for protein conjugation purposes.[47] However, our attempts to apply photocatalysis in live cell environments were

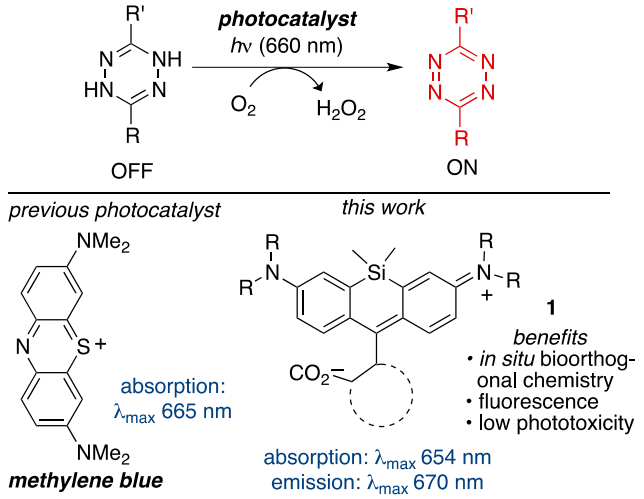

Figure 1. Photocatalytic oxidation of dihydrotetrazines with far-red light.

limited by issues of phototoxicity, presumably because methylene blue is also a strong sensitizer for singlet oxygen.

We queried whether far-red fluorescent dyes that are commonly used for applications in biology might find additional purpose as photocatalysts for inducing rapid bioorthogonal chemistry. Herein, we describe a mild, photocatalytic system for DHTz oxidation using Si-Rhodamine (SiR) derivatives **1**, which are water-soluble and absorb in the far-red range. While SiR dyes have previously been utilized as fluorophores for cellular and *in vivo* imaging[77−80] and as fluorogenic probes for detecting singlet oxygen,[81] they have not been used as photocatalysts. Here, we show that SiR derivatives efficiently and rapidly catalyze the oxidation of DHTz derivatives with greatly enhanced compatibility toward *trans*-cyclooctene dienophiles while also displaying enhanced cytocompatibility.

RESULTS AND DISCUSSION

Previously, we showed that the DHTz **2** (Figure 2A) could be oxidized to its corresponding Tz **3** under the action of photocatalysis or oxidation by HRP. Several dyes including methylene blue (660 nm), rose bengal (528 nm), and carboxyfluorescein (528 nm) were shown to be effective photocatalysts. As shown in Figure 2B, *in situ* monitoring of oxygen concentration during photocatalysis was used to provide evidence that O_2 is the terminal oxidant and that H_2O_2 is produced in a photocatalytic oxidation reaction. Thus, a solution of DHTz **2** (180 μM) in PBS was prepared, and the oxygen concentration was monitored using a Clark electrode. Here, 100% saturation at 25 °C represents 260 μM dissolved oxygen. Addition of catalytic quantities of rose bengal to DHTz **2** in the dark did not result in consumption of dissolved oxygen as seen in Figure 2B. Subsequent illumination at 528 nm over the course of 140 s lowers the oxygen level by 40% to 160 μM. Turning off the light caused the dissolved oxygen level to stabilize. Subsequently, catalase was added to effect the rapid dismutation of dissolved hydrogen peroxide, restoring approximately one-half of the oxygen originally depleted upon illumination of rose bengal. Subsequent illumination, now in the presence of catalase, depletes dissolved oxygen concentration at approximately one-half of the initial rate observed in the absence of catalase.

https://doi.org/10.1021/jacs.1c05547
J. Am. Chem. Soc. 2021, 143, 10793−10803

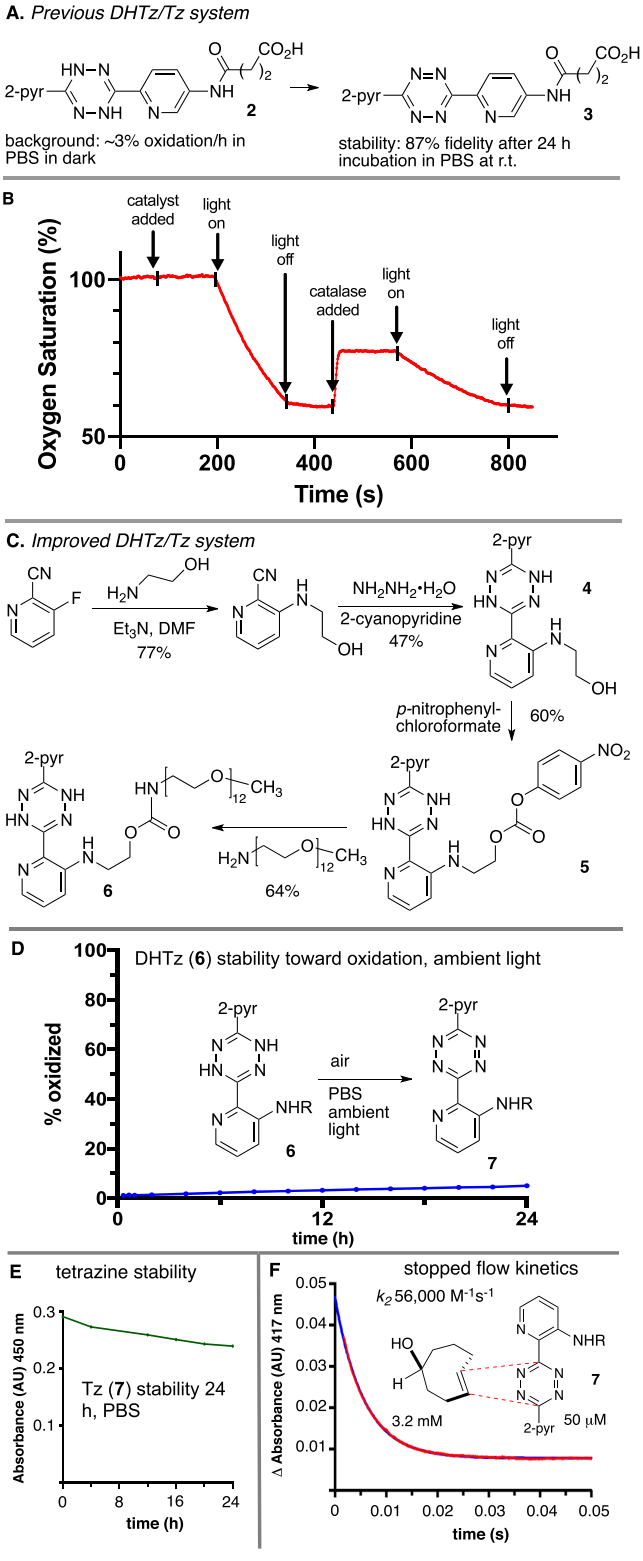

Figure 2. (A) Previous DHTz/Tz redox pair used for catalytic oxidation chemistry. (B) *In situ* monitoring of dissolved oxygen concentration demonstrates that O_2 is consumed and H_2O_2 is produced during photocatalytic DHTz oxidation. (C) Synthesis of a DHTz with improved stability in both the reduced and oxidized states. (D, E) Stability data in PBS, air, and ambient light for (D) DHTz **6** and (E) Tz **7** as monitored by tracking UV−vis absorption at 354 nm for **6** and by 450 nm for **7**. (F) Stopped-flow kinetics with UV monitoring was used to measure the rate of tetrazine ligation. Data is plotted in red, and the kinetic fit is in blue.

While DHTz **2** was highly resilient toward background oxidation in organic solvents, in PBS buffer the background oxidation of **2** to tetrazine **3** proceeded at a rate of ~3% conversion/h in PBS in the dark.[47] In ambient light, the rate of background oxidation was even faster. We sought to develop a more stable DHTz. Anticipating that a DHTz with an *ortho*-substituted aromatic group would be less susceptible to background oxidation, DHTz **4** and derivatives **5** and **6** were synthesized from 2-cyano-3-fluoropyridine via the route outlined in Figure 2C. The stability of water-soluble derivative **6** was studied by UV−vis spectroscopy, and the compound was found to be 95% stable after standing for 24 h in metal-free PBS buffer (Figure 2D).[82] Relative to **2**, Compound **6** also showed much improved stability in PBS containing 10% mouse serum, with 80% of **6** retained in the DHTz oxidation state after 24 h (Figure S28). Once oxidized, the stability of Tz **7** was similar to that of previously reported tetrazine **3**, with 80% of the tetrazine remaining after incubation for 24 h in PBS at room temperature (Figure 2E). In Diels−Alder chemistry, tetrazine **3** also displayed rapid kinetics with a second-rate constant of 56 000 ± 190 M^{-1} s^{-1} toward *axial*-5-hydroxy-*trans*-cyclooctene (Figures 2F, S29, and S30) that is of the same order of magnitude as the analogous reaction of **3** (80 200 ± 1700 M^{-1} s^{-1}, Figures S31 and S32).

Our initial studies revealed the incompatibility of methylene blue (MB) photocatalysis with *trans*-cyclooctene dienophiles. Photocatalysis was used to oxidize DHTz **6** to Tz **7** (Figure 3A). Low concentrations of MB (1 μM) converted 35 μM **6** to **7** upon irradiation with 660 nm light within 1.5 min. Reactions were monitored *in situ* using UV−vis spectroscopy, which showed DHTz **6** was formed in quantitative yield. Starting material **6** and product **7** have absorption maxima at 354 and 417 nm, respectively, and the spectra have an isosbestic point at 367 nm (Figure 3B). However, attempts to carry out the oxidation of **6** in the presence of TCO derivatives was marked by kinetically complex behavior. Moreover, a major limitation of the methylene blue system for photoactivation was revealed by irradiation of a solution of the 12-kDa protein thioredoxin (Trx) in the presence of methylene blue. As shown in Figure 3C, after 4 min far-red-light irradiation, the protein without MB still ionizes efficiently by HRMS with signal/noise (S/N) > 100. However, with the presence of MB (1 μM), the mass spectral quality of Trx decreased dramatically with $S/N < 10$. Similar oxidative damage was observed when either ribonuclease A (25 μM) or lysozyme (25 μM) was irradiated for 4 min with MB (1 μM) (Figure S57). These results illustrate the challenges associated with methylene blue-based photocatalysis with biological molecules.

As shown in Figure 4, SiR dyes were identified as novel, effective photocatalysts for DHTz oxidation with 660 nm light. Investigated were the analogs of the parent SiR dye **1a** (commercial from Spirochrome), fluorinated analog **1b**,[80] and the azetidine analogs **1c−e** developed at Janelia.[80] These dyes have maxima ranging from 643 to 669 nm. SiR dyes **1b−e** were chosen, as these dyes preferentially adopt the colored zwitterionic form and thus exhibit high absorptivity (ε > 100 000 M^{-1} cm^{-1}).[80] As shown in Figure 4A, all of these SiR dyes are effective photocatalysts. As shown in Figure 4B, the conversion of **6** to **7** was followed by *in situ* UV−vis spectroscopy by monitoring the reduction of absorption at 354 nm, λ_{max} for DHTz **6**. Conversion to product was light dependent, with complete conversion of 35 μM **6** to **7** in quantitative yield within 140 s when 1 μM of catalyst **1d** was used. The rate of conversion of **6** was not influenced by the addition of superoxide dismutase

https://doi.org/10.1021/jacs.1c05547
J. Am. Chem. Soc. 2021, 143, 10793−10803

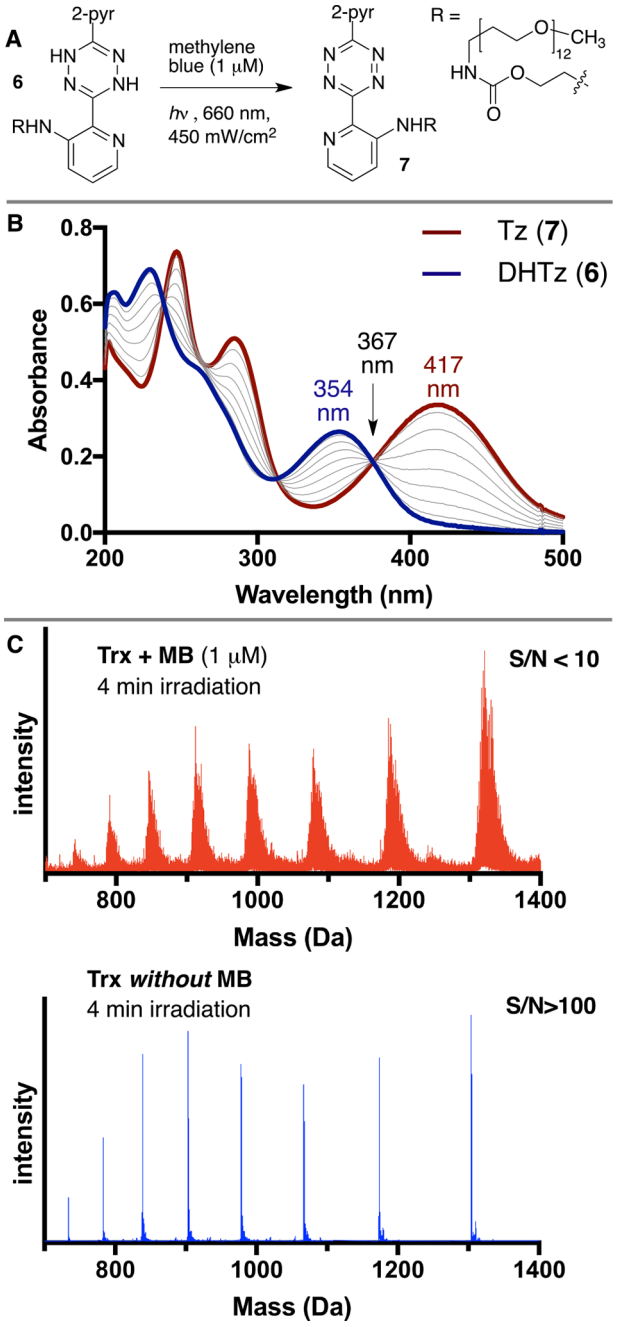

Figure 3. (A) Catalytic oxidation of **6** to **7** with methylene blue (MB) photocatalysis. (B) UV−vis spectroscopy was used to monitor reaction progress by following absorptions due to **6** (λ_{max} 354 nm) and **7** (λ_{max} 417 nm) relative to the isosbestic point at 367 nm. (C) Raw ESI mass spectra of the protein thioredoxin after 4 min irradiation with (top) and without (bottom) MB.

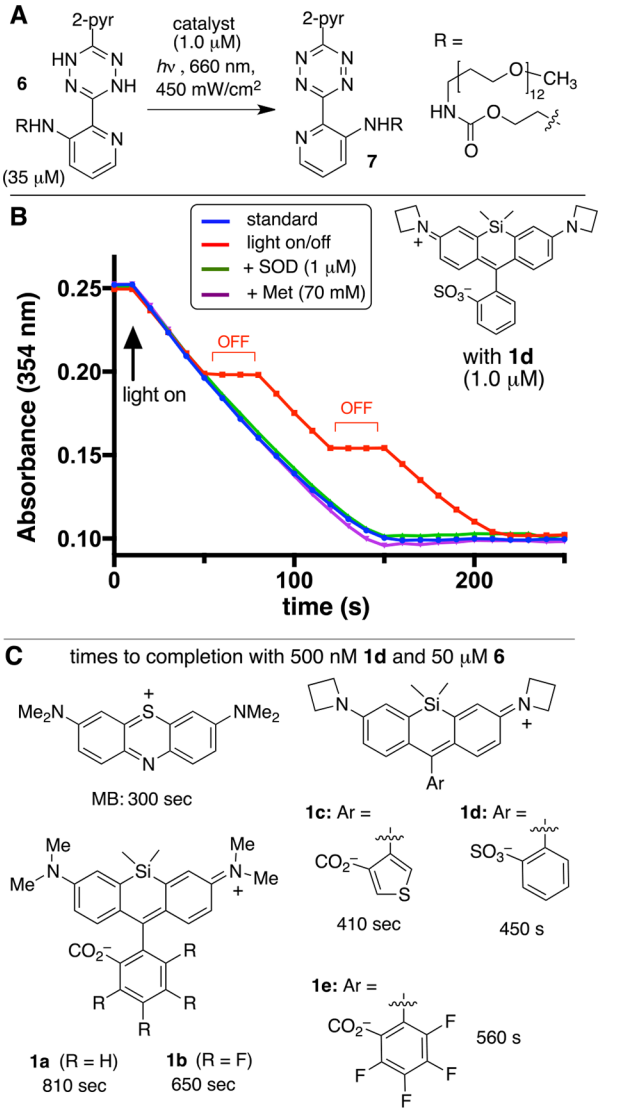

Figure 4. (A) Oxidation of DHTz **6** to **7** with SiR catalysts. (B) Oxidation of **6** to **7** catalyzed by **1d** is light dependent, and independent of quenchers of superoxide (SOD) and $^1O_2$ (methionine). (C) Rates of oxidation by MB and SiR catalysts.

(1 μM) nor the singlet oxygen scavenger[83] methionine (70 mM), suggesting that the mechanism of SiR-catalyzed DHTz oxidation occurs by a pathway that does not involve intermediacy of superoxide or singlet oxygen but instead involves direct sensitization of the DHTz by SiR, plausibly with electron transfer to the excited state of SiR.[84,85]

In a comparative study using 50 μM **6** and 500 nM of photocatalyst, all of the SiR dyes **1a−e** were effective photocatalysts that produced tetrazine **7** in >95% yield as judged by UV−vis spectroscopy in PBS (Figures 4C and S4). The fastest conversions were observed with the thiophene analog **1c** and benzenesulfonate **1d**, where completion was reached in 410 and 450 s, respectively, approaching the rates observed with methylene blue catalysis (300 s) under the same conditions.

Further mechanistic studies were carried out to provide additional details of SiR-catalyzed DHTz oxidation. An amplex-red assay for peroxide showed that H_2O_2 is a product of DHTz oxidation: starting with 30 μM **6**, 23 μM and 26 μM of H_2O_2 was detected under **1d**- and MB-photocatalysis, respectively (Figure S59). For photocatalysis by SiR **1d**, the rate of photooxidation increases proportionally with increasing light power density from 18 mW/cm^2 to 450 mW cm^2 (Figure S51). The rate of photooxidation also increases with increasing concentration of the SiR-catalyst **1d** (Figure S50) or with increasing DHTz concentration (Figure S52). However, as shown in Figure 4B and in Figures S50−S52, the kinetic behavior with respect to **6** is complex and cannot be described by a simple first-order or zero-order kinetic fit. Queries into whether the products formed were responsible for the anomalous kinetic behavior did not offer an explanation, as the rate is not influenced when the reaction

https://doi.org/10.1021/jacs.1c05547
J. Am. Chem. Soc. 2021, 143, 10793−10803

products H_2O_2 and Tz **7** are added separately or together, or if they are first generated *in situ* (Figures S54 and S55). Further inquiry into the intriguing kinetics of **1d** and the mechanistic details of the photocatalytic cycle are the subject of ongoing study.

To understand why SiR dyes are so much less detrimental than methylene blue in the oxidation of biomolecules, we probed the relative rates by which these dyes catalyze the production of singlet oxygen vs the DHTz oxidation. The water-soluble 9,10-anthracenediyl-bis(methylene)dimalonic acid (ABDA) was used as a singlet oxygen trap by monitoring of the disappearance of absorption at 402 nm. With methylene blue (2 μM), the rate of DHTz oxidation (100% conversion after 30 s at 35 μM DHTz) is comparable to the rate of singlet oxygen trapping (100% conversion after 20 s at 35 μM ABDA) (Figure S49). By contrast, with SiR catalyst **1d** (1 μM), the rate of DHTz oxidation (100% conversion after 3 min at 35 μM DHTz) is much more rapid than singlet oxygen trapping (100% conversion after 70 min at 35 μM ABDA) (Figure S49). For both SiR dyes (Figure 4) and methylene blue,[47] the rate of DHTz oxidation is not affected by the inclusion of a large excess of a singlet oxygen quencher, leading to the conclusion that the DHTz is not simply oxidized by singlet oxygen with either dye. It is possible that photocatalysis with SiR dyes differs by involving initial complexation with the DHTz. Concentration-dependent hypochromic and bathochromic shifts are observed in the long-wavelength band in the UV−vis spectrum upon mixing SiR **1d** with excess DHTz **6**. (Figure S53). Additional inquiry into the mechanism of SiR-catalyzed photooxidation is ongoing in our laboratories.

The ability of SiR **1d** to photocatalyze the oxidation of DHTz **6** with *in situ* protein conjugation was demonstrated as shown in Figures 5 and S6G−I. Protein conjugates of TCO (Figure S19), the cyclooctyne BCN (Figure S23), and the most reactive *trans*-cyclooctene, sTCO, were used to illustrate compatibility of several dienophiles with photocatalytic DHTz oxidation. As shown Figure 5A, single cysteine mutant of the protein thioredoxin (Trx-C32) was derivatized as the conjugate **Trx-sTCO**,[86] which does not react with DHTz **6** in the absence of light and/or photocatalyst. However, in the presence of 660 nm light (50 mW/cm^2) and photocatalyst **1d** (1 μM), *in situ* oxidation and Diels−Alder reaction proceeded efficiently to give conjugate **8** as determined by mass spectrometry (Figure 5B,C). Reaction progress was monitored by LC/MS, and the photoreaction stopped when Trx-sTCO was completely consumed after 15 min. As shown in Figure 5B, conversion to **8** was high, and as shown in Figure 5C, spectral quality was also high (S/N > 100) and did not suffer from singlet-oxygen-mediated degradation that was evident when Trx was irradiated in the presence of methylene blue (Figure 3C). Upon further irradiation in the presence of SiR **1d**, all of DHTz **6** was consumed, and consistent with the ability of SiR dyes to slowly sensitize singlet oxygen, oxidation products of conjugate **8** were slowly formed over the course of 4 h, as determined by mass spectrometry (Figures S16−S18).

Tetrazine ligation has been used for the creation of hydrogels for tissue engineering applications including *in vivo* cell delivery[87] and the creation of molecularly patterned matrices based on interfacial bioorthogonal chemistry.[88] Previously, Truong, Forsythe, and co-workers used our first-generation system (catalytic methylene blue, DHTz **2**, 660 nm light) via cross-linking with a 4-arm PEG-norbornene to encapsulate human mesenchymal stem cells (hMSCs); however, cell viability beyond day 1 was not described.[75] In our own experiments, the phototoxicity of methylene blue and the sensitivity of DHTz **2** under cell culture conditions have limited the broader application of our first-generation system for tissue engineering purposes.

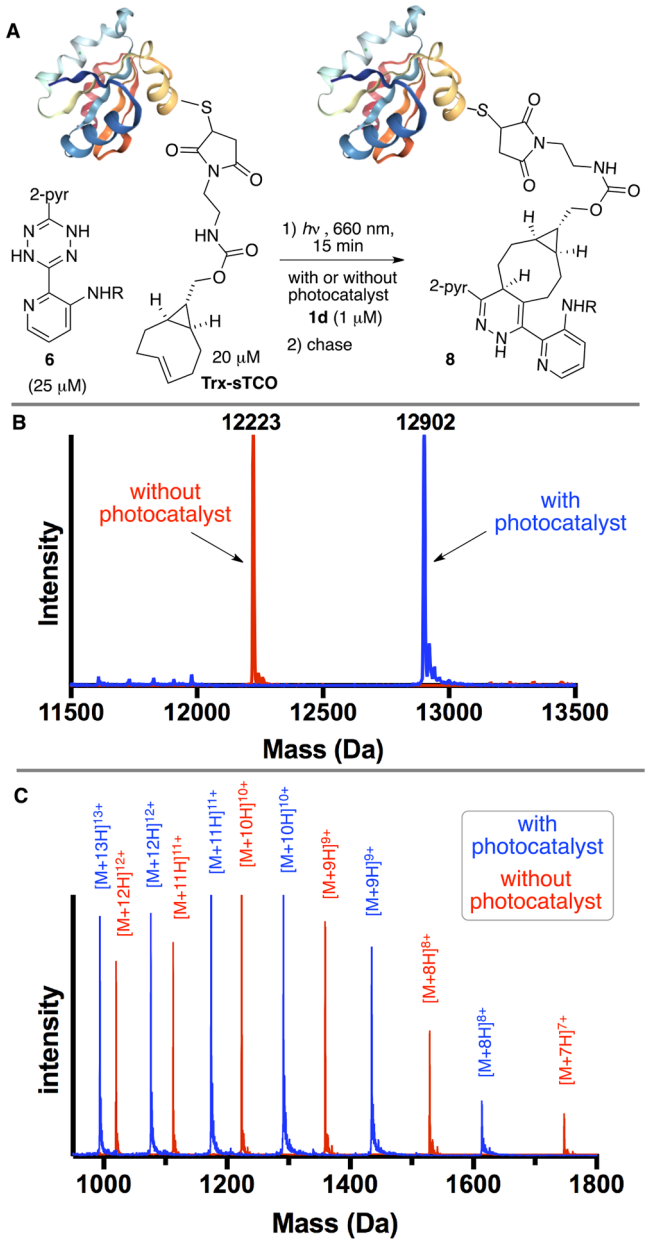

Figure 5. (A) Reaction of a thioredoxin−*trans*-cyclooctene conjugate (Trx-sTCO) with DHTz **6** proceeds efficiently in the presence of light and photocatalyst, but not if the catalyst or light is omitted. The reaction was carried out by exposing a solution of Trx-sTCO (20 μM) and **6** (25 μM) to 660 nm light (50 mW/cm^2) and photocatalyst **1d** (1 μM) for 15 min, followed by chasing with (4-(6-methyl-1,2,4,5-tetrazin-3-yl)phenyl)methanol to capture unreacted Trx-sTCO and MS analysis. (B) Deconvoluted and (C) raw mass spectra for the combination of **6** with Trx-sTCO with 660 nm light in the presence (blue) and absence (red) of photocatalyst **1d**. Product **8** is only formed in the presence of photocatalyst. For Trx, the calculated mass is 11 730.3 Da and the observed mass was 11 730 Da. Observed mass shifts relative to Trx were consistent with the calculated shifts for Trx-sTCO (+318.4 Da), **8** (+1171.4 Da), and the adduct of Trx-sTCO with (4-(6-methyl-1,2,4,5-tetrazin-3-yl)phenyl)methanol (+492.6 Da).

https://doi.org/10.1021/jacs.1c05547
J. Am. Chem. Soc. 2021, 143, 10793−10803

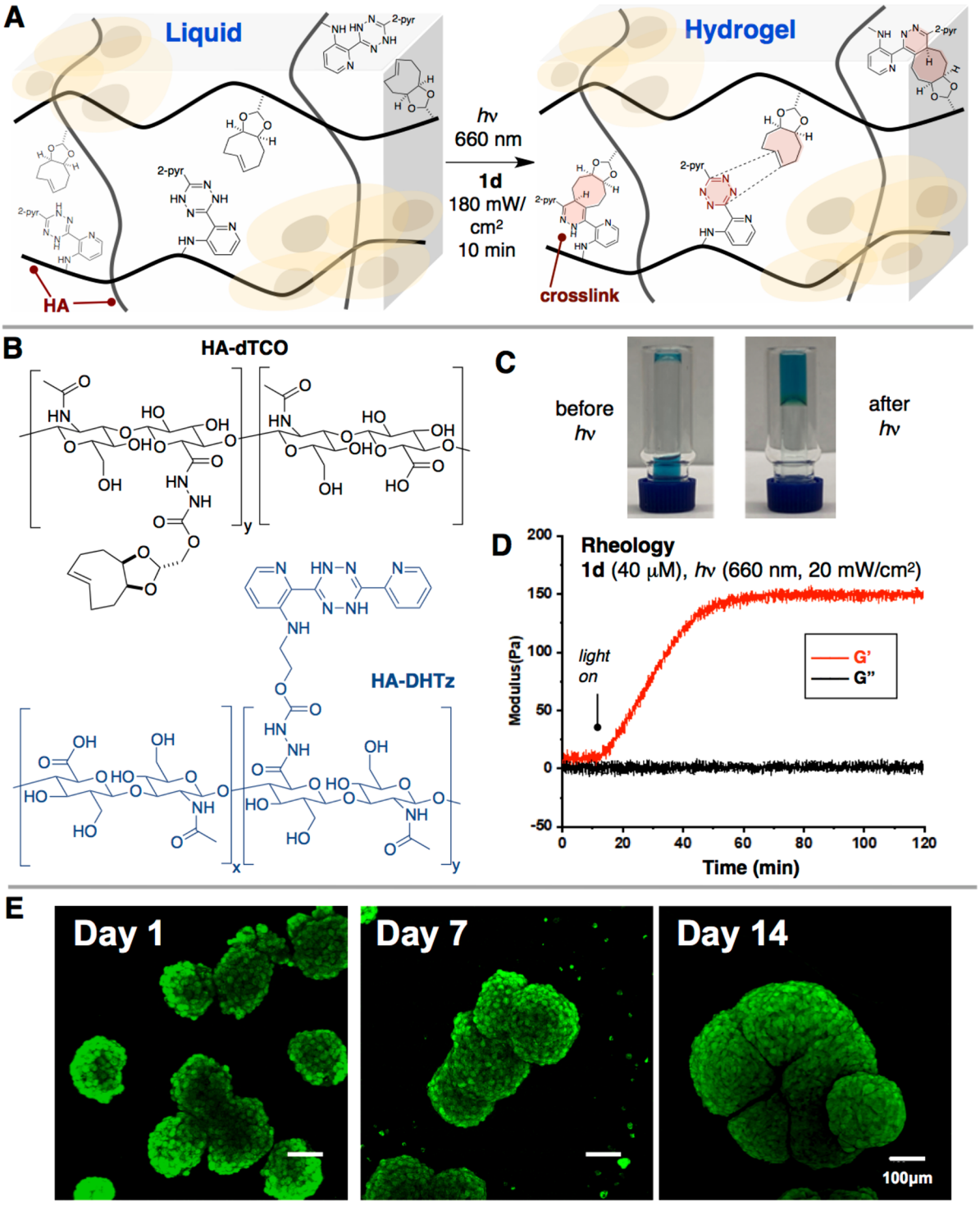

Figure 6. (A) Schematic description of red light photocatalytic turn-on of tetrazine ligation for cell encapsulation in HA hydrogels. (B) HA-dTCO (2.5 mM) and HA-DHTz (2 mM) were cross-linked by exposure to 660 nm light and catalyst **1d** (40 μM). (C) Vial inversion tests before and after irradiation, indicating transformation of a liquid to a hydrogel. The blue color is due to the SiR dye. (D) Representative rheological measurements of HA hydrogels prepared with 660 nm irradiation and SiR. For rheology, longer irradiation was required due to the lower intensity light source. (E) Confocal microscopy images of LNCaP spheroids after 1, 7, and 14 days of culture in HA hydrogels. Constructs were produced by irradiating a solution of HA-dTCO and HA-DHTz containing suspended cell spheroids. Live and dead cells were stained by calcein AM (green) and ethidium homodimer (red), respectively (both red and green channels are shown; isolated red and green channels shown in Figure S38). No dead cells were observed by microscopy.

As an illustration of the utility of SiR-photocatalyzed DHTz oxidation, we used catalyst **1d** in conjunction with far-red light to catalyze the formation of hyaluronic acid (HA)-based hydrogel matrices for 3D cell culture from a liquid cellular suspension. HA is a natural polysaccharide that is widely used to create hydrogels with desirable properties for drug delivery and tissue engineering applications.[89,90] As illustrated graphically in Figure 6A, we sought to initiate cross-linking of HA-derivatives

https://doi.org/10.1021/jacs.1c05547
J. Am. Chem. Soc. 2021, 143, 10793−10803

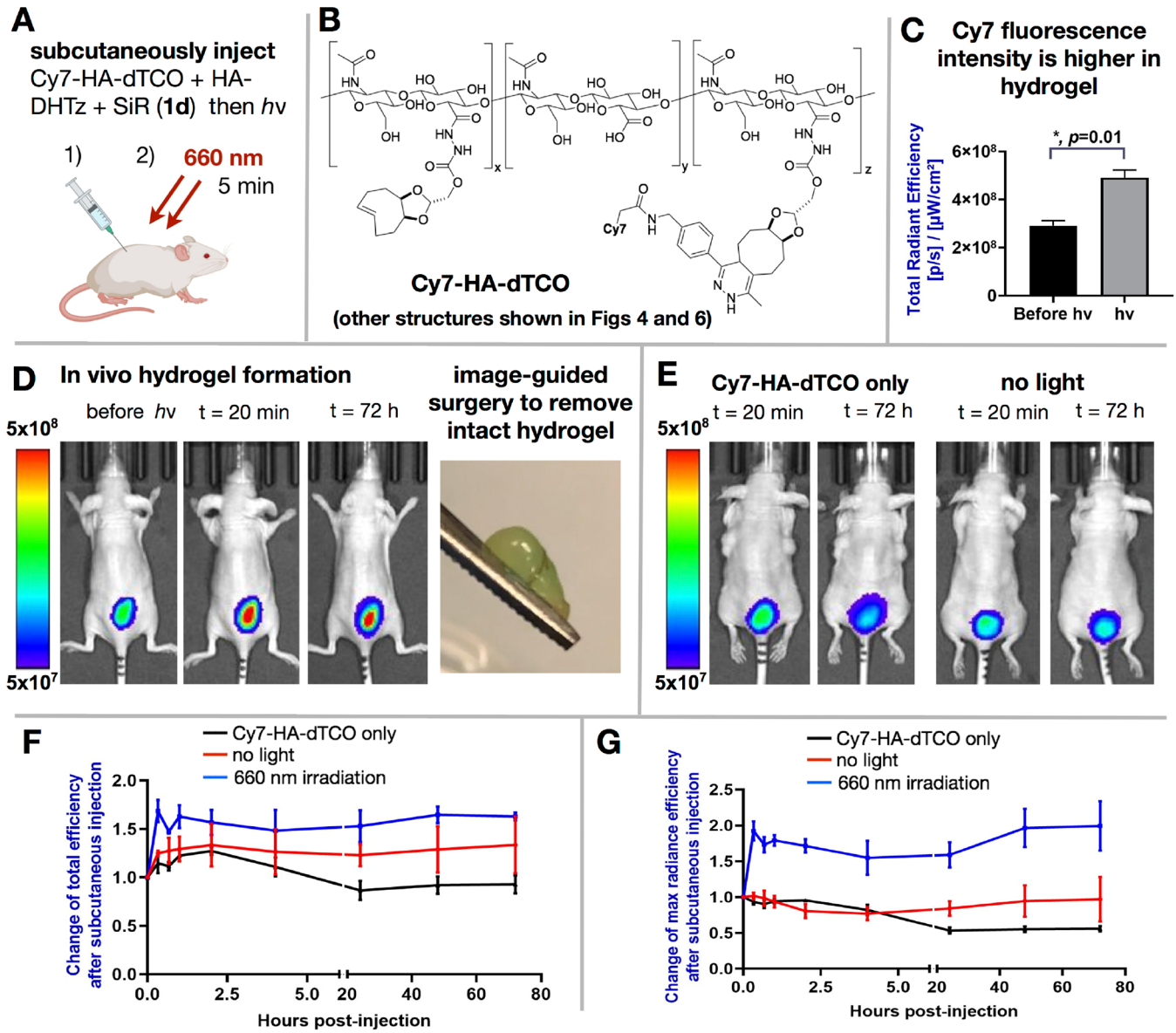

Figure 7. (A) Schematic description of procedure for injection/*in vivo* hydrogel formation. A solution of Cy7-HA-dTCO (2.5 mM), HA-DHTz (2 mM), SiR catalyst **1d** (40 μM), and catalase (10 μM) in PBS was injected subcutaneously in live mice and then irradiated for 5 min with 660 nm light. (B) Structure of Cy7-HA-dTCO, prepared by the conjugation of HA-dTCO with substoichiometric Cy7-tetrazine. (C) *In vitro* total radiant efficiency due to Cy7 in the mixture before and after illumination by 660 nm light. (D) Representative time-course images of animals that were subcutaneously injected with hydrogel precursor and illuminated with 660 nm light. The right image shows the hydrogel that was formed *in vivo* and removed surgically. (E) Control experiments where Cy7-HA-dTCO was injected, and where the hydrogel precursor solution was injected without illumination. (F, G) Plots showing the change in (F) maximum and (G) total radiant efficiency after subcutaneous injection.

bearing DHTz and TCO functionality upon irradiation at 660 nm in the presence of LNCaP prostate cancer spheroids using a SiR-photocatalyst. As shown in Figure 6B, dTCO- and DHTz-functionalized HA (**HA-dTCO** and **HA-DHTz**) were prepared using hydrazide linkers. Here, the dioxolane-fused dTCO was chosen due to its improved hydrophilicity relative to conventional TCO dienophiles.[48] As shown in Figure 6C, the hydrogel precursor solution was free-flowing before irradiation. After 10 min irradiation at 660 nm (180 mW/cm^2), a self-supporting hydrogel formed. Oscillatory rheology with *in situ* irradiation was then used to confirm hydrogel formation of the pre-gel solution of a desired formulation. As shown in Figure 6D, the storage modulus (G') increased noticeably upon the application of far-red light within 5 min, while the loss modulus (G'') remained unchanged. G' continued to increase while irradiation lasted, reaching the plateau of 150 ± 9 Pa after 60 min. No increase in G' was observed in the control experiments after 2 h, where either the light or photocatalyst was omitted from the rheology experiment, and only after 7 h did G' start to increase slightly (Figure S33). We note that the relatively long irradiation times for rheology studies were due to the low intensity (20 mW/cm^2) of the rheometer light source.

For 3D encapsulation studies, LNCaP spheroids with an average diameter of 100 μm, prepared following our established procedure,[91] were suspended in the pre-hydrogel solution. Catalase, an enzyme extensively present in humans and all organisms exposed to oxygen, was added as a co-catalyst to disproportionate the hydrogen peroxide generated by the photoreaction. Including catalase significantly improves cell viability, as isolated LNCaP cells irradiated for 10 min at 180

https://doi.org/10.1021/jacs.1c05547
J. Am. Chem. Soc. 2021, 143, 10793−10803

mW/cm^2 in the presence of **6** (2 mM DHTz), **1d** (40 μM), and catalase (2.5 mg/mL) show 94% (±2%) viability after 3 days (Figures S60 and S61), versus 39% (±16%) viability in controls that lacked catalase. Cell-laden hydrogels were created by irradiating the suspensions for 10 min at 180 mW/cm^2 in a Petri dish using a custom LED far-red-light source (Figure S34). Here, relatively short irradiation times were possible by direct irradiation at high power density without any detectable cell death. The resulting hydrogel constructs were cultured and imaged at varied time points by confocal microscopy. As shown in Figure 6E, live/dead staining followed by confocal microscopy showed that the LNCaP spheroids retained high viability throughout the cell culture experiment after 1, 7, and 14 days of culture.

The SiR-photocatalyzed tetrazine ligation was also used to create hydrogel materials in live mice by subcutaneous injection of a solution of SiR catalyst, **HA-DHTz**, and **HA-dTCO**, followed by brief irradiation with 660 nm light source (Figure 7A). To enable *in vivo* imaging, a NIR chromophore Cy7 was conjugated to **HA-dTCO** to give **Cy7-HA-dTCO** (20% dTCO and 0.5% Cy7 incorporation) (Figure 7B). A hydrogel precursor solution was then prepared by mixing **HA-DHTz** (2 mM), **Cy7-HA-dTCO** (2.5 mM), photocatalyst **1d** (40 μM), and catalase (10 μM). This resulting solution was a free-flowing, injectable liquid that was stable against background gelation even when allowed to stand in ambient light for 8 h. However, upon irradiation for 5 min with 660 nm light (530 mW/cm^2) a hydrogel formed rapidly. The resulting hydrogel showed a 70% increase in Cy7-fluorescence at 776 nm relative to the non-irradiated hydrogel precursor solution (Figure 7C). This increase in fluorescence quantum yield is the expected consequence of the dramatic viscosity increase upon gelation,[92] and the increase in fluorescence intensity served as a useful reporter of hydrogel formation *in vivo*. As shown in Figure 7D, subcutaneous injection of 0.04 mL of the hydrogel precursor solution in nude mice (female, 4−6 weeks old) was used to produce a fluorescent area with ∼6 mm diameter at the site of injection (Figure 7D). The fluorescence became significantly more intense upon 5 min irradiation at 660 nm, with immediate increases in maximum (+1.80-fold) and total (+1.91-fold) radiance efficiency that were persistent over the course of 72 h (Figure 7F,G). Complete time-course data is presented in Figure S42. In these animals, a visible bump on the skin due to *in vivo* hydrogel formation became apparent after irradiation (Figure S46). Image-guided surgery was conducted 20 min after irradiation, and a solid, fluorescent hydrogel was readily isolated (Figures 7D and S47). In control experiments where HA-DHTz was omitted and Diels−Alder cross-linking therefore impossible, there was no initial increase in maximum fluorescence intensity (Figure 7E,G) upon injection, and both the maximum and total fluorescence intensity decreased significantly over the course of 72 h (Figure 7F,G). In separate controls, the hydrogel precursor solution was injected, but 660 nm light was not applied. Again, no increase in fluorescence intensity was observed, but the signal was persistent over 72 h, suggesting that some gelation may have occurred. Image-guided surgery was also attempted 20 min post-injection. Unlike the experiment where 660 nm light was used, a viscoelastic solid was not formed, although a small amount of soft, sticky material was isolable (Figure S48). Thus, some gelation took place in the dark in the *in vivo* environment, perhaps due to DHTz oxidation at the gel interface to form a liquid-filled sac. For an injectable material, this background gelation should provide a practical advantage by increasing viscosity and holding the shape and position of the material prior to irradiation. However, photocuring with far-red light is necessary to create a stable, cross-linked hydrogel material *in vivo*.

CONCLUSIONS

SiR dyes, traditionally used as biological fluorophores, have been repurposed for applications in photocatalysis. With far-red light, SiR catalyzes the activation of rapid bioorthogonal chemistry through oxidation of a dihydrotetrazine to a tetrazine. A new dihydrotetrazine/tetrazine pair with high stability in both oxidation states is described. Of the SiR dyes studied, the Janelia Fluor-SiR dyes were found to be especially effective even at low catalyst loadings (typically 1 μM) with short irradiation times. Photocatalysis is successful in the presence of *trans*-cyclooctene dienophiles, and photocatalytic activation of a tetrazine was demonstrated on a site-selectively modified protein without signs of oxidative damage. SiR-based photocatalysis was used to cross-link aqueous solutions of hyaluronic acid polymers that were functionalized by dihydrotetrazine and *trans*-cyclooctenes, leading to hydrogels that can support 3D-cell culture. Photocatalysis was carried out *in vivo* in live mice through subcutaneous injection of a solution containing SiR photocatalyst and a Cy7-labeled hydrogel precursor, followed by irradiation with far-red light to create stable hydrogels *in vivo*. We anticipate that the activation of bioorthogonal chemistry through SiR photocatalysis will serve as a valuable tool for covalent bond formation with spatial temporal control in cellular and *in vivo* environments.

ASSOCIATED CONTENT

Supporting Information

The Supporting Information is available free of charge at https://pubs.acs.org/doi/10.1021/jacs.1c05547.

Synthetic procedures and compound characterization data; procedures for photochemical oxidation of dihydrotetrazines; procedures for protein expression, tagging, and modification; 3D-cell culture protocols and photochemical hydrogelation; and animal protocols and procedures for *in vivo* hydrogel formation (PDF)

AUTHOR INFORMATION

Corresponding Authors

Joseph M. Fox − *Department of Chemistry and Biochemistry and Department of Materials Science and Engineering, University of Delaware, Newark, Delaware 19716, United States;* orcid.org/0000-0002-8258-1640; Email: jmfox@udel.edu

Xinqiao Jia − *Department of Materials Science and Engineering, University of Delaware, Newark, Delaware 19716, United States; Delaware Biotechnology Institute, Newark, Delaware 19711, United States;* orcid.org/0000-0002-3564-5576; Email: xjia@udel.edu

Zibo Li − *Department of Radiology and Biomedical Research Imaging Center, University of North Carolina at Chapel Hill, Chapel Hill, North Carolina 27599, United States;* orcid.org/0000-0002-1063-0298; Email: zibo_li@med.unc.edu

https://doi.org/10.1021/jacs.1c05547
J. Am. Chem. Soc. 2021, 143, 10793−10803

Authors

Chuanqi Wang − *Department of Chemistry and Biochemistry, University of Delaware, Newark, Delaware 19716, United States*

He Zhang − *Department of Materials Science and Engineering, University of Delaware, Newark, Delaware 19716, United States;* orcid.org/0000-0003-1165-6702

Tao Zhang − *Department of Radiology and Biomedical Research Imaging Center, University of North Carolina at Chapel Hill, Chapel Hill, North Carolina 27599, United States*

Xiaoyu Zou − *Department of Materials Science and Engineering, University of Delaware, Newark, Delaware 19716, United States*

Hui Wang − *Department of Radiology and Biomedical Research Imaging Center, University of North Carolina at Chapel Hill, Chapel Hill, North Carolina 27599, United States*

Julia E. Rosenberger − *Department of Chemistry and Biochemistry, University of Delaware, Newark, Delaware 19716, United States*

Raghu Vannam − *Department of Chemistry and Biochemistry, University of Delaware, Newark, Delaware 19716, United States;* orcid.org/0000-0002-6665-8548

William S. Trout − *Department of Chemistry and Biochemistry, University of Delaware, Newark, Delaware 19716, United States*

Jonathan B. Grimm − *Janelia Research Campus, Howard Hughes Medical Institute, Ashburn, Virginia 20147, United States;* orcid.org/0000-0003-0331-4200

Luke D. Lavis − *Janelia Research Campus, Howard Hughes Medical Institute, Ashburn, Virginia 20147, United States;* orcid.org/0000-0002-0789-6343

Colin Thorpe − *Department of Chemistry and Biochemistry, University of Delaware, Newark, Delaware 19716, United States;* orcid.org/0000-0001-8238-0112

Complete contact information is available at: https://pubs.acs.org/10.1021/jacs.1c05547

Author Contributions

#C.W. and H.Z. contributed equally.

Notes

The authors declare no competing financial interest.

■ ACKNOWLEDGMENTS

This work was supported by NIH (R01GM132460, R01DC014461), NSF (DMR1809612, OISE1844463), Pfizer, and the State of Delaware CAT grant program. Instrumentation was supported by NIH awards P20GM104316, S10OD025185, S10OD026951, S10OD016267, and DMR-2011824.

■ REFERENCES

(1) Nicewicz, D. A.; Nguyen, T. M. Recent Applications of Organic Dyes as Photoredox Catalysts in Organic Synthesis. *ACS Catal.* **2014**, *4*, 355−360.

(2) Li, P.; Terrett, J. A.; Zbieg, J. R. Visible-Light Photocatalysis as an Enabling Technology for Drug Discovery: A Paradigm Shift for Chemical Reactivity. *ACS Med. Chem. Lett.* **2020**, *11*, 2120−2130.

(3) Romero, N. A.; Nicewicz, D. A. Organic Photoredox Catalysis. *Chem. Rev.* **2016**, *116*, 10075−10166.

(4) Geri, J. B.; Oakley, J. V.; Reyes-Robles, T.; Wang, T.; McCarver, S. J.; White, C. H.; Rodriguez-Rivera, F. P.; Parker, D. L.; Hett, E. C.; Fadeyi, O. O.; Oslund, R. C.; MacMillan, D. W. C. Microenvironment Mapping via Dexter Energy Transfer on Immune Cells. *Science* **2020**, *367*, 1091.

(5) Alabugin, A. Near-IR Photochemistry for Biology: Exploiting the Optical Window of Tissue. *Photochem. Photobiol.* **2019**, *95*, 722−732.

(6) Nani, R. R.; Gorka, A. P.; Nagaya, T.; Yamamoto, T.; Ivanic, J.; Kobayashi, H.; Schnermann, M. J. In Vivo Activation of Duocarmycin-Antibody Conjugates by Near-Infrared Light. *ACS Cent. Sci.* **2017**, *3*, 329−337.

(7) Palao, E.; Slanina, T.; Muchova, L.; Solomek, T.; Vitek, L.; Klan, P. Transition-Metal-Free CO-Releasing BODIPY Derivatives Activatable by Visible to NIR Light as Promising Bioactive Molecules. *J. Am. Chem. Soc.* **2016**, *138*, 126−133.

(8) Lobo, A. C. S.; Silva, A. D.; Tomé, V. A.; Pinto, S. M. A.; Silva, E. F. F.; Calvete, M. J. F.; Gomes, C. M. F.; Pereira, M. M.; Arnaut, L. G. Phthalocyanine Labels for Near-Infrared Fluorescence Imaging of Solid Tumors. *J. Med. Chem.* **2016**, *59*, 4688−4696.

(9) Al-Afyouni, M. H.; Rohrabaugh, T. N.; Al-Afyouni, K. F.; Turro, C. New Ru(ii) photocages operative with near-IR light: new platform for drug delivery in the PDT window. *Chem. Sci.* **2018**, *9*, 6711−6720.

(10) Chilakamarthi, U.; Giribabu, L. Photodynamic Therapy: Past, Present and Future. *Chem. Record* **2017**, *17*, 775−802.

(11) Ye, S.; Cui, C.; Cheng, X.; Zhao, M.; Mao, Q.; Zhang, Y.; Wang, A.; Fang, J.; Zhao, Y.; Shi, H. Red Light-Initiated Cross-Linking of NIR Probes to Cytoplasmic RNA: An Innovative Strategy for Prolonged Imaging and Unexpected Tumor Suppression. *J. Am. Chem. Soc.* **2020**, *142*, 21502−21512.

(12) Devaraj, N. K. The Future of Bioorthogonal Chemistry. *ACS Cent. Sci.* **2018**, *4*, 952−959.

(13) Nguyen, S. S.; Prescher, J. A. Developing Bioorthogonal Probes to Span a Spectrum of Reactivities. *Nat. Rev.* **2020**, *4*, 476−489.

(14) van Onzen, A. H. A. M.; Versteegen, R. M.; Hoeben, F. J. M.; Filot, I. A. W.; Rossin, R.; Zhu, T.; Wu, J.; Hudson, P. J.; Janssen, H. M.; ten Hoeve, W.; Robillard, M. S. Bioorthogonal Tetrazine Carbamate Cleavage by Highly Reactive trans-Cyclooctene. *J. Am. Chem. Soc.* **2020**, *142*, 10955−10963.

(15) Li, J.; Jia, S.; Chen, P. R. Diels-Alder reaction-triggered bioorthogonal protein decaging in living cells. *Nat. Chem. Biol.* **2014**, *10*, 1003−1005.

(16) Versteegen, R. M.; Rossin, R.; Ten Hoeve, W.; Janssen, H. M.; Robillard, M. S. Click to Release: Instantaneous Doxorubicin Elimination upon Tetrazine Ligation. *Angew. Chem., Int. Ed.* **2013**, *52*, 14112−14116.

(17) Tu, J.; Xu, M.; Parvez, S.; Peterson, R. T.; Franzini, R. M. Bioorthogonal Removal of 3-Isocyanopropyl Groups Enables the Controlled Release of Fluorophores and Drugs in Vivo. *J. Am. Chem. Soc.* **2018**, *140*, 8410−8414.

(18) Wilkovitsch, M.; Haider, M.; Sohr, B.; Herrmann, B.; Klubnick, J.; Weissleder, R.; Carlson, J. C. T.; Mikula, H. A Cleavable C2-Symmetric trans-Cyclooctene Enables Fast and Complete Bioorthogonal Disassembly of Molecular Probes. *J. Am. Chem. Soc.* **2020**, *142*, 19132−19141.

(19) Carlson, J. C. T.; Mikula, H.; Weissleder, R. Unraveling Tetrazine-Triggered Bioorthogonal Elimination Enables Chemical Tools for Ultrafast Release and Universal Cleavage. *J. Am. Chem. Soc.* **2018**, *140*, 3603−3612.

(20) Jiménez-Moreno, E.; Guo, Z.; Oliveira, B. L.; Albuquerque, I. S.; Kitowski, A.; Guerreiro, A.; Boutureira, O.; Rodrigues, T.; Jiménez-Osés, G.; Bernardes, G. J. L. Vinyl Ether/Tetrazine Pair for the Traceless Release of Alcohols in Cells. *Angew. Chem., Int. Ed.* **2017**, *56*, 243−247.

(21) Wu, H.; Alexander, S. C.; Jin, S.; Devaraj, N. K. A Bioorthogonal Near-Infrared Fluorogenic Probe for mRNA Detection. *J. Am. Chem. Soc.* **2016**, *138*, 11429−11432.

(22) Lelieveldt, L. P. W. M.; Eising, S.; Wijen, A.; Bonger, K. M. Vinylboronic acid-caged prodrug activation using click-to-release tetrazine ligation. *Org. Biomol. Chem.* **2019**, *17*, 8816−8821.

(23) Herner, A.; Lin, Q. Photo-Triggered Click Chemistry for Biological Applications. *Top. Curr. Chem.* **2016**, *374*, 1.

(24) Tasdelen, M. A.; Yagci, Y. Light-Induced Click Reactions. *Angew. Chem., Int. Ed.* **2013**, *52*, 5930−5938.
(25) Song, W.; Wang, Y.; Qu, J.; Madden, M. M.; Lin, Q. A photoinducible 1,3-dipolar cycloaddition reaction for rapid, selective modification of tetrazole-containing proteins. *Angew. Chem., Int. Ed.* **2008**, *47*, 2832−2835.
(26) An, P.; Lewandowski, T. M.; Erbay, T. G.; Liu, P.; Lin, Q. Sterically Shielded, Stabilized Nitrile Imine for Rapid Bioorthogonal Protein Labeling in Live Cells. *J. Am. Chem. Soc.* **2018**, *140*, 4860−4868.
(27) Yu, Z.; Lin, Q. Design of Spiro[2.3]hex-1-ene, a Genetically Encodable Double-Strained Alkene for Superfast Photoclick Chemistry. *J. Am. Chem. Soc.* **2014**, *136*, 4153−4156.
(28) Mayer, S. V.; Murnauer, A.; Wrisberg, M. K.; Jokisch, M. L.; Lang, K. Photo-induced and Rapid Labeling of Tetrazine-Bearing Proteins via Cyclopropenone-Caged Bicyclononynes. *Angew. Chem., Int. Ed.* **2019**, *58*, 15876−15882.
(29) Mcnitt, C. D.; Cheng, H.; Ullrich, S.; Popik, V. V.; Bjerknes, M. Multiphoton Activation of Photo-Strain-Promoted Azide Alkyne Cycloaddition "Click" Reagents Enables in Situ Labeling with Submicrometer Resolution. *J. Am. Chem. Soc.* **2017**, *139*, 14029−14032.
(30) Poloukhtine, A. A.; Mbua, N. E.; Wolfert, M. A.; Boons, G. J.; Popik, V. V. Selective labeling of living cells by a photo-triggered click reaction. *J. Am. Chem. Soc.* **2009**, *131*, 15769−15776.
(31) Sutton, D. A.; Popik, V. V. Sequential Photochemistry of Dibenzo[a, e]dicyclopropa[c, g][8]annulene-1,6-dione: Selective Formation of Didehydrodibenzo[a, e][8]annulenes with Ultrafast SPAAC Reactivity. *J. Org. Chem.* **2016**, *81*, 8850−8857.
(32) Shah, L.; Laughlin, S. T.; Carrico, I. S. Light-Activated Staudinger-Bertozzi Ligation within Living Animals. *J. Am. Chem. Soc.* **2016**, *138*, 5186−5189.
(33) Shete, A. U.; El-Zaatari, B. M.; French, J. M.; Kloxin, C. J. Blue-light activated rapid polymerization for defect-free bulk Cu(i)-catalyzed azide-alkyne cycloaddition (CuAAC) crosslinked networks. *Chem. Commun.* **2016**, *52*, 10574−10577.
(34) Lim, R. K. V.; Lin, Q. Azirine ligation: fast and selective protein conjugation via photoinduced azirine-alkene cycloaddition. *Chem. Commun.* **2010**, *46*, 7993−7995.
(35) Gann, A. W.; Amoroso, J. W.; Einck, V. J.; Rice, W. P.; Chambers, J. J.; Schnarr, N. A. A photoinduced, benzyne click reaction. *Org. Lett.* **2014**, *16*, 2003−2005.
(36) Gao, J.; Xiong, Q.; Wu, X.; Deng, J.; Zhang, X.; Zhao, X.; Deng, P.; Yu, Z. Direct ring-strain loading for visible-light accelerated bioorthogonal ligation via diarylsydnone-dibenzo[b, f][1,4,5]-thiadiazepine photo-click reactions. *Commun. Chem.* **2020**, *3*, 29.
(37) Zhang, L.; Zhang, X.; Yao, Z.; Jiang, S.; Deng, J.; Li, B.; Yu, Z. Discovery of Fluorogenic Diarylsydnone-Alkene Photoligation: Conversion of ortho-Dual-Twisted Diarylsydnones into Planar Pyrazolines. *J. Am. Chem. Soc.* **2018**, *140*, 7390−7394.
(38) Li, J.; Kong, H.; Huang, L.; Cheng, B.; Qin, K.; Zheng, M.; Yan, Z.; Zhang, Y. Visible Light-Initiated Bioorthogonal Photoclick Cycloaddition. *J. Am. Chem. Soc.* **2018**, *140*, 14542−14546.
(39) Li, J.; Kong, H.; Zhu, C.; Zhang, Y. Photo-controllable bioorthogonal chemistry for spatiotemporal control of bio-targets in living systems. *Chem. Sci.* **2020**, *11*, 3390−3396.
(40) Bruins, J. J.; Albada, B.; van Delft, F. ortho-Quinones and Analogues Thereof: Highly Reactive Intermediates for Fast and Selective Biofunctionalization. *Chem. - Eur. J.* **2018**, *24*, 4749−4756.
(41) Bruins, J. J.; Blanco-Ania, D.; Van Der Doef, V.; Van Delft, F. L.; Albada, B. Orthogonal, dual protein labelling by tandem cycloaddition of strained alkenes and alkynes to ortho-quinones and azides. *Chem. Commun.* **2018**, *54*, 7338−7341.
(42) Arumugam, S.; Popik, V. V. Photochemical Generation and the Reactivity ofo-Naphthoquinone Methides in Aqueous Solutions. *J. Am. Chem. Soc.* **2009**, *131*, 11892−11899.
(43) Feist, F.; Rodrigues, L. L.; Walden, S. L.; Krappitz, T. W.; Dargaville, T. R.; Weil, T.; Goldmann, A. S.; Blinco, J. P.; Barner-Kowollik, C. Light-induced Ligation of o-Quinodimethanes with Gated Fluorescence Self-reporting. *J. Am. Chem. Soc.* **2020**, *142*, 7744−7748.
(44) Bruins, J. J.; Westphal, A. H.; Albada, B.; Wagner, K.; Bartels, L.; Spits, H.; Van Berkel, W. J. H.; Van Delft, F. L. Inducible, Site-Specific Protein Labeling by Tyrosine Oxidation-Strain-Promoted (4 + 2) Cycloaddition. *Bioconjugate Chem.* **2017**, *28*, 1189−1193.
(45) Singh, K.; Fennell, C. J.; Coutsias, E. A.; Latifi, R.; Hartson, S.; Weaver, J. D. Light Harvesting for Rapid and Selective Reactions: Click Chemistry with Strain-Loadable Alkenes. *Chem.* **2018**, *4*, 124−137.
(46) Yu, Z.; Ohulchanskyy, T. Y.; An, P.; Prasad, P. N.; Lin, Q. Fluorogenic, Two-Photon-Triggered Photoclick Chemistry in Live Mammalian Cells. *J. Am. Chem. Soc.* **2013**, *135*, 16766−16769.
(47) Zhang, H.; Trout, W. S.; Liu, S.; Andrade, G. A.; Hudson, D. A.; Scinto, S. L.; Dicker, K. T.; Li, Y.; Lazouski, N.; Rosenthal, J.; Thorpe, C.; Jia, X.; Fox, J. M. Rapid Bioorthogonal Chemistry Turn-on through Enzymatic or Long Wavelength Photocatalytic Activation of Tetrazine Ligation. *J. Am. Chem. Soc.* **2016**, *138*, 5978−5983.
(48) Darko, A.; Wallace, S.; Dmitrenko, O.; Machovina, M. M.; Mehl, R. A.; Chin, J. W.; Fox, J. M. Conformationally Strained trans-Cyclooctene with Improved Stability and Excellent Reactivity in Tetrazine Ligation. *Chem. Sci.* **2014**, *5*, 3770−3776.
(49) Selvaraj, R.; Fox, J. M. trans-Cyclooctene–a stable, voracious dienophile for bioorthogonal labeling. *Curr. Opin. Chem. Biol.* **2013**, *17*, 753−760.
(50) Wu, H.; Devaraj, N. K. Inverse Electron-Demand Diels-Alder Bioorthogonal Reactions. *Top. Curr. Chem.* **2016**, *374*, 3.
(51) Wu, H.; Devaraj, N. K. Advances in Tetrazine Bioorthogonal Chemistry Driven by the Synthesis of Novel Tetrazines and Dienophiles. *Acc. Chem. Res.* **2018**, *51*, 1249−1259.
(52) Kumar, P.; Zainul, O.; Camarda, F. M.; Jiang, T.; Mannone, J. A.; Huang, W.; Laughlin, S. T. Caged Cyclopropenes with Improved Tetrazine Ligation Kinetics. *Org. Lett.* **2019**, *21*, 3721−3725.
(53) Jiang, T.; Kumar, P.; Huang, W.; Kao, W. S.; Thompson, A. O.; Camarda, F. M.; Laughlin, S. T. Modular Enzyme- and Light-Based Activation of Cyclopropene-Tetrazine Ligation. *ChemBioChem* **2019**, *20*, 2222−2226.
(54) Selvaraj, R.; Fox, J. M. An efficient and mild oxidant for the synthesis of s-tetrazines. *Tetrahedron Lett.* **2014**, *55*, 4795−4797.
(55) Ehret, F.; Wu, H.; Alexander, S. C.; Devaraj, N. K. Electrochemical Control of Rapid Bioorthogonal Tetrazine Ligations for Selective Functionalization of Microelectrodes. *J. Am. Chem. Soc.* **2015**, *137*, 8876−8879.
(56) Min, D. J.; Miomandre, F.; Audebert, P.; Kwon, J. E.; Park, S. Y. s-Tetrazines as a New Electrode-Active Material for Secondary Batteries. *ChemSusChem* **2019**, *12*, 503−510.
(57) Nickerl, G.; Senkovska, I.; Kaskel, S. Tetrazine functionalized zirconium MOF as an optical sensor for oxidizing gases. *Chem. Commun.* **2015**, *51*, 2280−2282.
(58) Liu, L.; Zhang, D.; Johnson, M.; Devaraj, N. K. Light-activated tetrazines enable live-cell spatiotemporal control of bioorthogonal reactions. *bioRxiv* **2020**, DOI: 10.1101/2020.12.01.405423.
(59) Haines, L. A.; Rajagopal, K.; Ozbas, B.; Salick, D. A.; Pochan, D. J.; Schneider, J. P. Light-Activated Hydrogel Formation via the Triggered Folding and Self-Assembly of a Designed Peptide. *J. Am. Chem. Soc.* **2005**, *127*, 17025−17029.
(60) Arkenberg, M. R.; Nguyen, H. D.; Lin, C.-C. Recent advances in bio-orthogonal and dynamic crosslinking of biomimetic hydrogels. *J. Mater. Chem. B* **2020**, *8*, 7835−7855.
(61) Prestwich, G. D. Hyaluronic acid-based clinical biomaterials derived for cell and molecule delivery in regenerative medicine. *J. Controlled Release* **2011**, *155*, 193−199.
(62) Wu, H.-D.; Yang, J.-C.; Tsai, T.; Ji, D.-Y.; Chang, W.-J.; Chen, C.-C.; Lee, S.-Y. Development of a chitosan-polyglutamate based injectable polyelectrolyte complex scaffold. *Carbohydr. Polym.* **2011**, *85*, 318−324.
(63) Xu, Q.; Guo, L.; A, S.; Gao, Y.; Zhou, D.; Greiser, U.; Creagh-Flynn, J.; Zhang, H.; Dong, Y.; Cutlar, L.; Wang, F.; Liu, W.; Wang, W.; Wang, W. Injectable hyperbranched poly(beta-amino ester) hydrogels with on-demand degradation profiles to match wound healing processes. *Chem. Sci.* **2018**, *9*, 2179−2187.

(64) DeForest, C. A.; Polizzotti, B. D.; Anseth, K. S. Sequential click reactions for synthesizing and patterning three-dimensional cell microenvironments. *Nat. Mater.* **2009**, *8*, 659−664.
(65) Skardal, A.; Murphy, S. V.; Crowell, K.; Mack, D.; Atala, A.; Soker, S. A tunable hydrogel system for long-term release of cell-secreted cytokines and bioprinted in situ wound cell delivery. *J. Biomed. Mater. Res., Part B* **2017**, *105*, 1986−2000.
(66) Lim, K. S.; Klotz, B. J.; Lindberg, G. C. J.; Melchels, F. P. W.; Hooper, G. J.; Malda, J.; Gawlitta, D.; Woodfield, T. B. F. Visible Light Cross-Linking of Gelatin Hydrogels Offers an Enhanced Cell Microenvironment with Improved Light Penetration Depth. *Macromol. Biosci.* **2019**, *19*, No. e1900098.
(67) Meng, Z.; Zhou, X.; Xu, J.; Han, X.; Dong, Z.; Wang, H.; Zhang, Y.; She, J.; Xu, L.; Wang, C.; Liu, Z. Light-Triggered In Situ Gelation to Enable Robust Photodynamic-Immunotherapy by Repeated Stimulations. *Adv. Mater.* **2019**, *31*, No. e1900927.
(68) Brown, T. E.; Anseth, K. S. Spatiotemporal hydrogel biomaterials for regenerative medicine. *Chem. Soc. Rev.* **2017**, *46*, 6532−6552.
(69) Xu, X.; Farach-Carson, M. C.; Jia, X. Three-dimensional in vitro tumor models for cancer research and drug evaluation. *Biotechnol. Adv.* **2014**, *32*, 1256−1268.
(70) Xu, X.; Sabanayagam, C. R.; Harrington, D. A.; Farach-Carson, M. C.; Jia, X. A hydrogel-based tumor model for the evaluation of nanoparticle-based cancer therapeutics. *Biomaterials* **2014**, *35*, 3319−3330.
(71) Ding, J.; Yao, Y.; Li, J.; Duan, Y.; Nakkala, J. R.; Feng, X.; Cao, W.; Wang, Y.; Hong, L.; Shen, L.; Mao, Z.; Zhu, Y.; Gao, C. A Reactive Oxygen Species Scavenging and O2 Generating Injectable Hydrogel for Myocardial Infarction Treatment In vivo. *Small* **2020**, *16*, 2005038.
(72) Cui, L.; Vivona, S.; Smith, B. R.; Kothapalli, S.-R.; Liu, J.; Ma, X.; Chen, Z.; Taylor, M.; Kierstead, P. H.; Fréchet, J. M. J.; Gambhir, S. S.; Rao, J. Reduction Triggered In Situ Polymerization in Living Mice. *J. Am. Chem. Soc.* **2020**, *142*, 15575−15584.
(73) Boase, N. R. B. Shining a Light on Bioorthogonal Photochemistry for Polymer Science. *Macromol. Rapid Commun.* **2020**, *41*, 2000305.
(74) Carthew, J.; Frith, J. E.; Forsythe, J. S.; Truong, V. X. Polyethylene glycol-gelatin hydrogels with tuneable stiffness prepared by horseradish peroxidase-activated tetrazine-norbornene ligation. *J. Mater. Chem. B* **2018**, *6*, 1394−1401.
(75) Truong, V. X.; Tsang, K. M.; Ercole, F.; Forsythe, J. S. Red Light Activation of Tetrazine-Norbornene Conjugation for Bioorthogonal Polymer Cross-Linking across Tissue. *Chem. Mater.* **2017**, *29*, 3678−3685.
(76) Liu, Z.; Lv, Y.; Zhu, A.; An, Z. One-Enzyme Triple Catalysis: Employing the Promiscuity of Horseradish Peroxidase for Synthesis and Functionalization of Well-Defined Polymers. *ACS Macro Lett.* **2018**, *7*, 1−6.
(77) Fu, M.; Xiao, Y.; Qian, X.; Zhao, D.; Xu, Y. A design concept of long-wavelength fluorescent analogs of rhodamine dyes: replacement of oxygen with silicon atom. *Chem. Commun.* **2008**, 1780−1782.
(78) Koide, Y.; Urano, Y.; Hanaoka, K.; Terai, T.; Nagano, T. Evolution of Group 14 Rhodamines as Platforms for Near-Infrared Fluorescence Probes Utilizing Photoinduced Electron Transfer. *ACS Chem. Biol.* **2011**, *6*, 600−608.
(79) Koide, Y.; Urano, Y.; Hanaoka, K.; Piao, W.; Kusakabe, M.; Saito, N.; Terai, T.; Okabe, T.; Nagano, T. Development of NIR Fluorescent Dyes Based on Si-rhodamine for in Vivo Imaging. *J. Am. Chem. Soc.* **2012**, *134*, 5029−5031.
(80) Grimm, J. B.; Brown, T. A.; Tkachuk, A. N.; Lavis, L. D. General Synthetic Method for Si-Fluoresceins and Si-Rhodamines. *ACS Cent. Sci.* **2017**, *3*, 975−985.
(81) Kim, S.; Tachikawa, T.; Fujitsuka, M.; Majima, T. Far-Red Fluorescence Probe for Monitoring Singlet Oxygen during Photodynamic Therapy. *J. Am. Chem. Soc.* **2014**, *136*, 11707−11715.
(82) To remove adventitous metal impurities, PBS buffer was purified by filtration through chelex resin prior to use.
(83) Devasagayam, T. P. A.; Sundquist, A. R.; Di Mascio, P.; Kaiser, S.; Sies, H. Activity of thiols as singlet molecular oxygen quenchers. *J. Photochem. Photobiol., B* **1991**, *9*, 105−116.
(84) Lincoln, R.; Greene, L. E.; Krumova, K.; Ding, Z.; Cosa, G. Electronic Excited State Redox Properties for BODIPY Dyes Predicted from Hammett Constants: Estimating the Driving Force of Photoinduced Electron Transfer. *J. Phys. Chem. A* **2014**, *118*, 10622−10630.
(85) Heinlein, T.; Knemeyer, J.-P.; Piestert, O.; Sauer, M. Photoinduced Electron Transfer between Fluorescent Dyes and Guanosine Residues in DNA-Hairpins. *J. Phys. Chem. B* **2003**, *107*, 7957−7964.
(86) Taylor, M. T.; Blackman, M. L.; Dmitrenko, O.; Fox, J. M. Design and synthesis of highly reactive dienophiles for the tetrazine-trans-cyclooctene ligation. *J. Am. Chem. Soc.* **2011**, *133*, 9646−9649.
(87) Koshy, S. T.; Desai, R. M.; Joly, P.; Li, J.; Bagrodia, R. K.; Lewin, S. A.; Joshi, N. S.; Mooney, D. J. Click-Crosslinked Injectable Gelatin Hydrogels. *Adv. Healthcare Mater.* **2016**, *5*, 541−547.
(88) Dicker, K. T.; Moore, A. C.; Garabedian, N. T.; Zhang, H.; Scinto, S. L.; Akins, R. E.; Burris, D. L.; Fox, J. M.; Jia, X. Spatial Patterning of Molecular Cues and Vascular Cells in Fully Integrated Hydrogel Channels via Interfacial Bioorthogonal Cross-Linking. *ACS Appl. Mater. Interfaces* **2019**, *11*, 16402−16411.
(89) Ozdemir, T.; Fowler, E. W.; Liu, S.; Harrington, D. A.; Witt, R. L.; Farach-Carson, M. C.; Pradhan-Bhatt, S.; Jia, X. Tuning Hydrogel Properties to Promote the Assembly of Salivary Gland Spheroids in 3D. *ACS Biomater. Sci. Eng.* **2016**, *2*, 2217−2230.
(90) Zhang, H.; Dicker, K. T.; Xu, X.; Jia, X.; Fox, J. M. Interfacial Bioorthogonal Cross-Linking. *ACS Macro Lett.* **2014**, *3*, 727−731.
(91) Ozdemir, T.; Srinivasan, P. P.; Zakheim, D. R.; Harrington, D. A.; Witt, R. L.; Farach-Carson, M. C.; Jia, X.; Pradhan-Bhatt, S. Bottom-up assembly of salivary gland microtissues for assessing myoepithelial cell function. *Biomaterials* **2017**, *142*, 124−135.
(92) Sharafy, S.; Muszkat, K. A. Viscosity dependence of fluorescence quantum yields. *J. Am. Chem. Soc.* **1971**, *93*, 4119−4125.

https://doi.org/10.1021/jacs.1c05547
J. Am. Chem. Soc. 2021, 143, 10793−10803